ANALYSIS OF ICED AEROFOIL PERFORMANCE USING CFD CODES

N. P. Dart and P. O'Brien

Defence Evaluation and Research Agency
Farnborough, United Kingdom

Abstract

This paper addresses the problem of the aerodynamic degradation of helicopter rotors by ice accretion, focusing on the potential role for CFD (computational fluid dynamics) codes in the prediction of helicopter performance in icing conditions. An initial investigation has been conducted to assess the accuracy of current CFD methods to determine the aerodynamic characteristics of iced aerofoils. A Navier-Stokes flow solver and a viscous-inviscid interaction program were chosen to perform a computational analysis of the flow about a NACA 0012 aerofoil with simulated glaze ice. Lift, drag and pressure coefficient comparisons are made with experimental data for the clean and iced aerofoil. Discrepancies that exist between the results are discussed, and conclusions are drawn on the possible direction of future work in this area.

Nomenclature

α - Aerofoil incidence
C_D - Drag coefficient
Note: $C_D = 0.0001 = 1$ drag count
C_L - Lift coefficient
C_P - Pressure coefficient
M   - Mach number
R   - Reynolds number

Introduction

Icing occurs when a helicopter enters a cloud containing super-cooled water droplets. These droplets are deposited on the surface of the helicopter and form ice. A particular hazard occurs when ice accretes on the leading edge of the rotor blades, causing a number of performance, vibration, and safety problems. This paper will focus on helicopter performance degradation that occurs during icing by studying the aerodynamic characteristics of aerofoils with ice accretions.

Effects of ice accretions on aerofoil performance

Accretion of ice on aerofoils can cause a very significant rise in profile drag (figure 1), resulting in a corresponding increase in the rotor torque required to maintain a given flight condition. The aerofoil
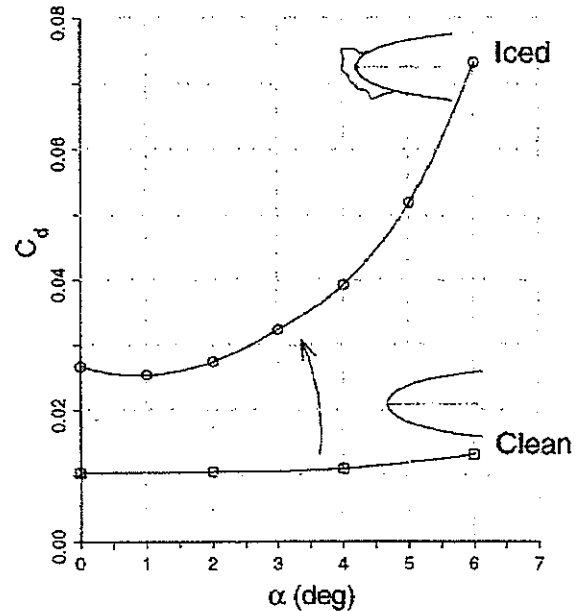
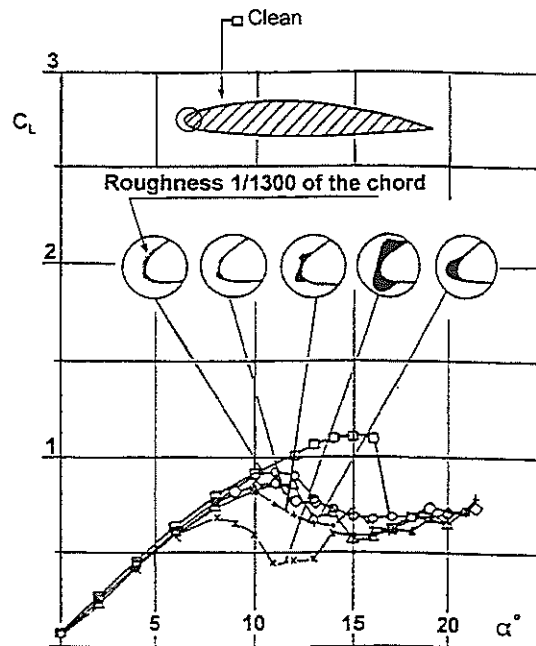Figure 1. Typical effect of an ice accretion on the drag coefficient of an aerofoil.

Figure 2. Typical effect of an ice accretion on the lift coefficient of an aerofoil (taken from Ref. 1).

107.1

maximum lift coefficient may also be affected adversely (figure 2), causing effects such as premature retreating blade stall and hence a reduction in the flight envelope.

Adverse changes to the aerofoil pitching moment may also occur, but since these will affect the rotor control forces rather than the aerodynamic performance of the rotor, changes to the pitching moment will not be considered during this investigation.

The performance of iced aerofoils is very sensitive to the shape and roughness of the ice accretion. Different types of ice accretions can form on helicopter blades depending on the atmospheric and flight conditions. These can be categorised into three main types (figure 3).

a) Rime Icing

Temperature,
Airspeed or LWC
Increasing
↓

b) Glaze Icing

Temperature
or Airspeed
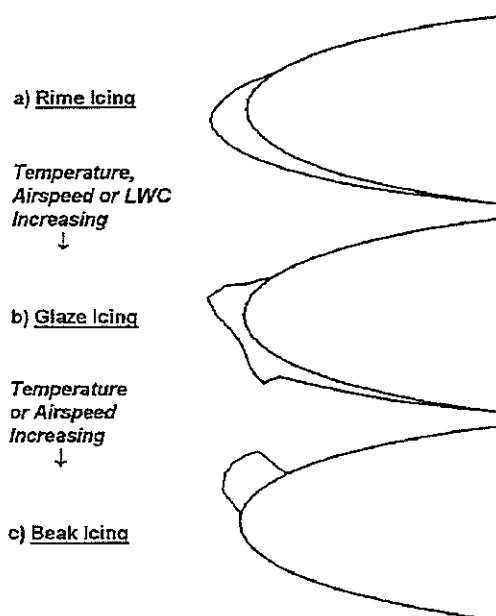Increasing
↓

c) Beak Icing

Figure 3. Main categories of ice accretion that
form on helicopter rotor blades

Rime ice forms when all of the impinging water droplets freeze instantaneously on the surface of the aerofoil. Consequently, a streamlined ice accretion forms that results in a relatively low aerodynamic performance penalty.

Glaze ice is produced when the atmospheric or flight conditions are such that only a fraction of the impinging water freezes, and the remainder runs backwards as a liquid water film along the aerofoil. A higher rate of freezing tends to occur either side of the stagnation point, resulting in characteristic ice 'horns'. These bluff ice horns disrupt the airflow and cause a severe degradation to the aerodynamic performance of the aerofoil.

Beak ice tends to form towards the outer radius of the rotor blade. In this region, sufficient kinetic

heating may exist at the stagnation line to prevent freezing, and the liquid water film can only freeze in the upper surface low pressure region where surface temperatures are reduced by adiabatic expansion of the airflow.

It is also important to note that a very slight ice contamination, resulting in a change to the surface roughness, but no obvious change to the aerofoil geometry, can be sufficient to create a noticeable performance degradation.

In summary, the magnitude of the aerofoil performance degradation is highly dependent on the shape of the ice accretion. The ice thickness, the thickness distribution, the location of the ice accretion, and the surface roughness of the ice all have a significant effect on the aerodynamic characteristics. The type of aerofoil is also a significant factor that affects its sensitivity to icing. For example, an aerofoil designed to maintain laminar flow in clean air will experience a much higher drag rise during light icing than a conventional aerofoil in the same conditions.

As noted, the shape and size of an ice accretion is dependent on a number of atmospheric and flight parameters:

- Aerofoil size and shape
- Outside air temperature
- Airspeed
- Cloud liquid water content
- Exposure time
- Cloud water droplet size

Given such a large number of variables, the number of possible combinations, and hence ice shapes, is very large. Consequently, it is impracticable to generate empirical correlations to predict the ice shape and performance degradation that would occur for an arbitrary icing encounter. Experimental testing or, in recent years, the use of analytical computer codes is required to evaluate the shape of the ice accretion that forms under given conditions. Previous research (eg. Ref. 2) has produced helicopter performance prediction methods for flight in icing, using empirical correlations for iced aerofoil performance characteristics, based on experimental data. However, these methods have a limited accuracy and applicability.

The long term objective is to produce an overall performance prediction code for helicopters that integrates accurate modelling of ice accretion with CFD techniques for aerofoil performance analysis.

Description of the Theoretical Models

Selection of the theoretical models

Three CFD codes were used in this investigation, namely BVGK (Ref. 3), N2DVC (Ref. 4) and

CITY3D. BVGK is a viscous-inviscid interaction program developed by the Defence Evaluation and Research Agency (DERA), designed to predict the aerodynamic characteristics of an aerofoil in transonic flow. N2DVC, also produced by DERA, is a Navier-Stokes flow solver capable of calculating viscous flows by solving the steady Reynolds-averaged Navier-Stokes equations. Limited results from CITY3D, an unsteady Navier-Stokes code, written at City University, London, are also presented in this paper. These codes are considered to be representative of the current relevant CFD capabilities for aerofoil analysis.
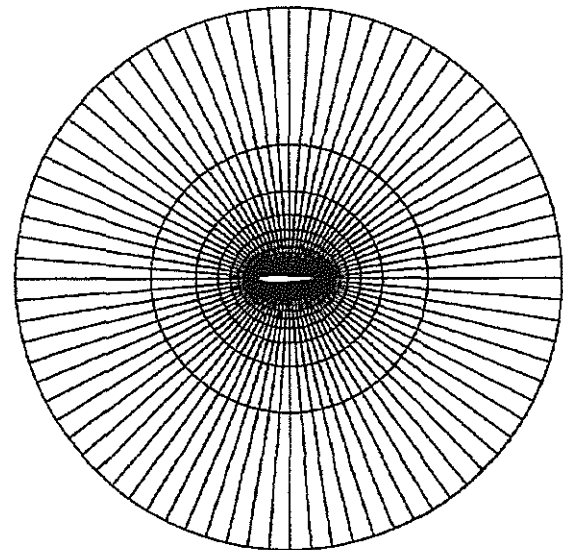
Description of BVGK

BVGK is an enhanced version of VGK (Viscous Garabedian and Korn program, Ref. 5), a computer package for predicting the aerodynamic characteristics of a two dimensional single element aerofoil immersed in a subsonic freestream, with allowances for the effects of viscosity and shock waves. Development of BVGK in 1987 (Ref. 3) allowed accurate solutions to be predicted for cases where small regions of separated flow existed around the aerofoil. The code consists of two components: a grid generator and a flow solver.

The program commences with the generation of the computational grid around the aerofoil using a conformal mapping scheme which transforms the aerofoil into the inside of a circle of unit radius. The grid usually has dimensions of 160×30 (160 radial grid lines and 30 concentric). An example is shown in figure 4.

The method employed by the flow solver couples finite difference solutions for inviscid flow about the aerofoil with solutions for the displacement effects of the boundary layer and wake. The basic equations governing the inviscid flow element in BVGK are the full potential equations for steady compressible flow of a gas (Ref. 5). Unlike conventional full potential schemes, the finite difference method utilised by BVGK (which is termed partially-conservative) has been developed to predict flows with shock waves. The viscous flow element consists of integral methods for the laminar and turbulent boundary layer components. The displacement and momentum thickness distributions are calculated allowing for the effects of the pressures obtained from the inviscid flow element.

The advantage of a viscous-inviscid flow solver is that the effects of viscosity are not considered in regions where the flow generally behaves as an inviscid fluid. The method is therefore more computationally efficient than a Navier-Stokes flow solver, and potentially beneficial for applications where multiple flow calculations would be required (such as in a helicopter blade element computer code).

(a) View of the full grid (only half of the grid lines are shown for clarity)
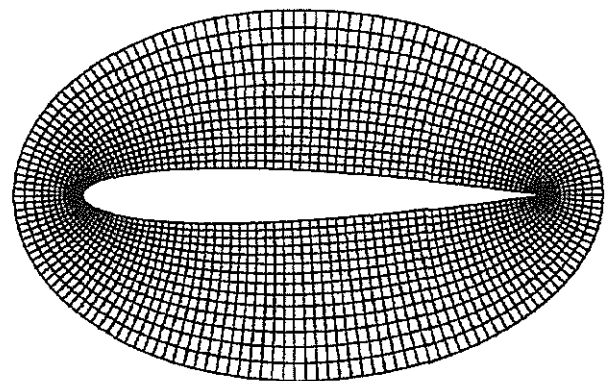
(b) View of the grid in the vicinity of the aerofoil

Figure 4. A typical grid produced by BVGK

Description of the N2DVC Navier-Stokes Flow Solver

The flow solver N2DVC calculates a finite-volume approximation to the two-dimensional steady Reynolds-averaged Navier-Stokes equations. The finite-volume discretisation of the equations is known as the Vertex-Centroid method. This method is formally second-order accurate in space and uses matrix artificial dissipation for control of spurious modes and clean capture of shock waves. The method currently uses a Baldwin-Lomax turbulence model, which is suitable for the calculation of equilibrium turbulent flows. This model has been extensively investigated in the literature and has been found to provide a poor predictive capability for flows containing significant regions of separation. In addition, the method is a steady-state solver so that it cannot predict unsteady behaviour such as unsteady separations and vortex shedding.

A more complete description of the method can be found in reference 3.

Description of the CITY3D Navier-Stokes Flow Solver

CITY3D is normally used for civil engineering applications but has been employed to provide a prediction of the aerodynamic characteristics of iced aerofoils. The code is a finite-volume flow solver developed, in part, with support from DERA-Farnborough. It solves the three-dimensional unsteady Navier-Stokes equations in a strongly-conservative, primitive-variable formulation. The equations are cast in general, coordinate independent forms, and are solved on non-orthogonal meshes generated in a multiblock, block-structured fashion. A co-located storage arrangement is employed. The code is only valid for incompressible flows and utilises a pressure-correction method to couple the iterative solutions of the velocity and pressure fields. Spatial discretisation is by choice of first and second-order accurate schemes (Upwind and MINMOD, respectively) while temporal discretisation is first-order Euler. Turbulence modelling is by either two-equation, eddy-viscosity closure or by a complete Reynolds-stress transport model. The former consists of the $k-\varepsilon$ model in both its standard and RNG formulation, the latter is based on the SSG pressure-strain model which has proved quite useful for flows in complex domains. The high Reynolds-number forms of both models are used, the assumption being that the flow under consideration is turbulent everywhere. Thus no laminar-turbulence transition is allowed and the flow adjacent to a solid boundary is assumed to obey a standard logarithmic law of the wall distribution.

Test Cases

When ice forms on an aerofoil, the surface of the accretion is irregular. This is illustrated by figure 5 which shows the cross section of a typical glaze ice accretion. It was beyond the capability of the available grid generators to map a geometry such as this exactly. Smoothing of the ice accretion surface coordinates to some degree was therefore needed prior to running the grid generator.
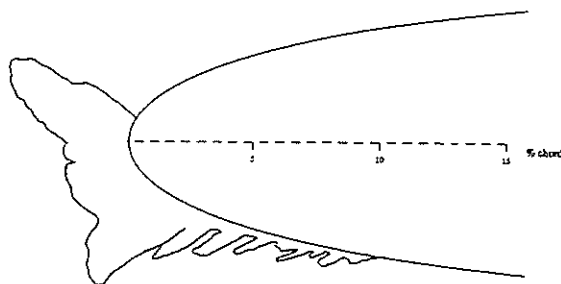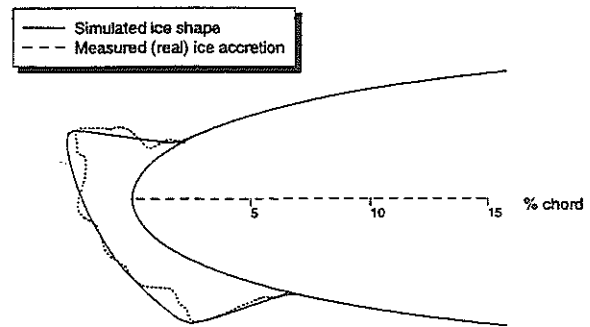
Figure 5. A typical ice accretion

Figure 6. The simulated ice shape selected for this investigation and the measured ice shape on which it was modelled.

Angle of attack	4°
Airspeed	58.1m/s
M_	0.178
Droplet diameter	20μm
Liquid Water Content	2.1g/m³
Static air temperature	-7.8°C
Exposure time	5 minutes
Chord	0.533m

Table 1. Test conditions for the icing experiment on which the simulated ice shape was based.

To overcome this inherent problem, a simulated ice shape was selected for this study. Its shape was based on an actual ice accretion (figure 6) which was grown in an icing wind tunnel at the test conditions shown in table 1 (taken from reference 6). The simulated accretion has none of the small scale irregularities of the actual accretion, but maintains the major features of its shape. Consequently, this profile can be used without the need for smoothing, ensuring equivalence between the geometry tested experimentally, and that modelled using the CFD codes. In addition, an extensive programme of dry wind tunnels tests has been conducted on this simulated accretion (references 6-10) providing an experimental database for use in comparisons with theory.

Additional glaze ice profiles were also chosen for this study during the early stages of the project. However, initial calculations were troublesome and problems were encountered with the grid generation around the irregular shape of the real ice profiles. The only solution was significant smoothing of the ice profile, which was considered to have an unacceptable effect on the aerodynamics and therefore introduced an additional element of uncertainty into the investigation. Consequently, it was decided that these real ice shapes would not be used in the present investigation. A rime ice shape was not selected because such accretions are

generally more streamlined than glaze accretions and would not test the limitations of the CFD codes. Since a glaze ice shape is considered to have the 'worst case' geometry from the CFD viewpoint, only the simulated glaze accretion was used in this study.

Results and Discussion

BVGK Results

Clean aerofoil

Initial tests were conducted on the clean NACA 0012 profile. BVGK was used to predict drag and lift coefficients for a range of incidences at the conditions used during the experiment described and presented in reference 6 ($M = 0.12$, $R = 1.5 \times 10^6$). In figures 7 and 8, the results are plotted against experimentally measured values taken from reference 6. It can be seen that BVGK predictions compare well with the experimental results, although problems were encountered obtaining a converged solution at an incidence of 6° and above. The reason for this could not be established although it was speculated that since the program has been developed to give accurate solutions for transonic flows at relatively high Reynolds numbers, it might not be optimised or well suited for use at the low Mach and Reynolds numbers used for the tests.
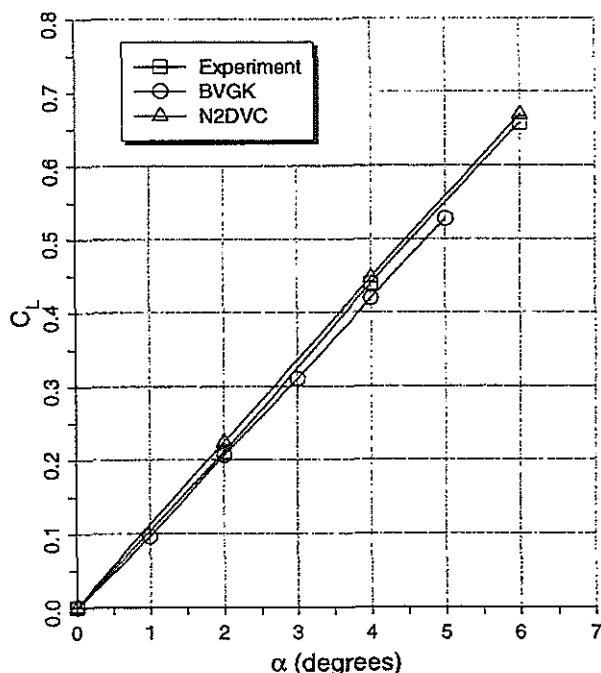

Figure 7. Comparison between the lift coefficients measured for a clean NACA 0012 aerofoil and values predicted by the CFD codes.
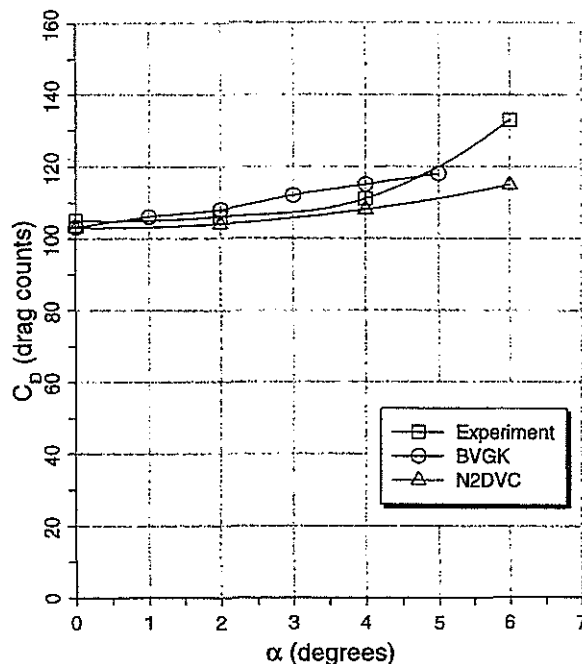

Figure 8. Comparison between the drag coefficients measured for a clean NACA 0012 aerofoil and values predicted by the CFD codes.

Iced Aerofoil

Using BVGK to assess the aerodynamic characteristics of the iced aerofoil was more difficult than for the clean aerofoil. Problems were first encountered with the grid generating element. Although this executed without producing any run-time errors, upon closer inspection, the grid was found to be badly generated with several of the concentric grid lines crossing inside the aerofoil surface. Not surprisingly, the flow solving element of BVGK then failed to obtain a solution.

Modifications were made to the BVGK grid generating routine which then allowed the geometry to be successfully mapped. This was done by inserting a relaxation factor into the iterative mapping scheme which eliminated the oscillations in the mapping solution which were causing the problems, thus allowing convergence. However, a flow solution could still not be obtained, and the iterative sequence quickly diverged. A number of parameters were changed in an effort to prevent the divergence. Relaxation factors were reduced, boundary layer transition points were moved, and the flow calculations were started at a milder flow condition (lower aerofoil incidence). However, none of these changes allowed the code to run successfully.

An inviscid run was successfully carried out using BVGK at an aerofoil incidence of 4°. Although the inviscid flow solution has little use in the prediction of aerofoil drag, it does give important information

about the pressure gradients around the aerofoil, so that regions of separation can be predicted. Information from the inviscid run showed that a very high suction peak occurs with the inviscid flow around the upper ice horn, with a minimum pressure coefficient value of about -19. Such an extreme inviscid flow is thought to cause difficulties with the boundary layer calculation method when the two are coupled, and hence prevent successful use of the code in the viscous mode.

Experimental results (Ref. 7) for the iced aerofoil have shown that large separation bubbles exist at all angles of attack on the upper and lower surface. Since BVGK is only capable of calculating flows with small areas of separation, it was concluded that the flow around the iced aerofoil was too severe for BVGK to predict.

Faired Aerofoil

Further attempts were made to run BVGK with the iced aerofoil by including a fairing at the interface between the ice and the aerofoil to prevent the high suction peak from forming. It was decided that the best opportunity of obtaining an accurate solution from BVGK would if this pseudo-surface were allowed to follow the extent of the natural separation bubbles that exist on the upper and lower surfaces. The shapes of these separation bubbles have been determined experimentally (Ref. 7). The separation bubble measured for the 4° incidence case was chosen for the aerofoil coordinate modification because the shape of the iced aerofoil is based on an ice accretion grown at an angle of attack of 4°. Figure 9 shows the modified aerofoil geometry.
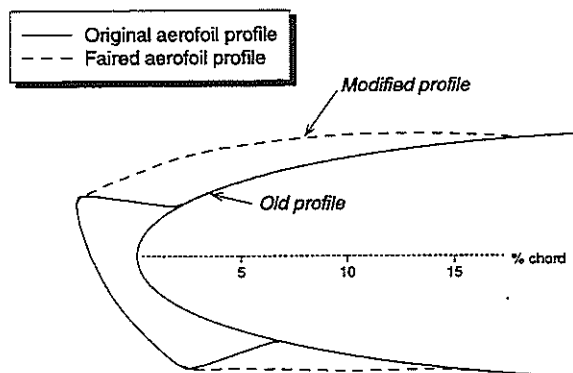

Figure 9. Modifications made to the aerofoil profile to include a fairing between the ice and aerofoil

Despite these changes to the aerofoil geometry, the flow solution quickly diverged at a Reynolds number of 1.5×10^6 (the flow condition used in the experimental test). Reducing the iterative relaxation

factors and moving the boundary layer transition points had little positive effect on the convergence. Increasing the Reynolds number to 3×10^6 and 6×10^6 allowed a flow solution to be obtained for low angles of attack, but a successful run for the 4° incidence case could only be achieved using a Reynolds number of 9×10^6. The results from BVGK at this flow condition are illustrated in figures 10 and 11, showing comparisons with the experimental lift and drag values. It should be noted that the validity of the BVGK results at incidences other than at 4° is limited because the modified aerofoil geometry is only representative of the separation bubbles that exist at 4°.
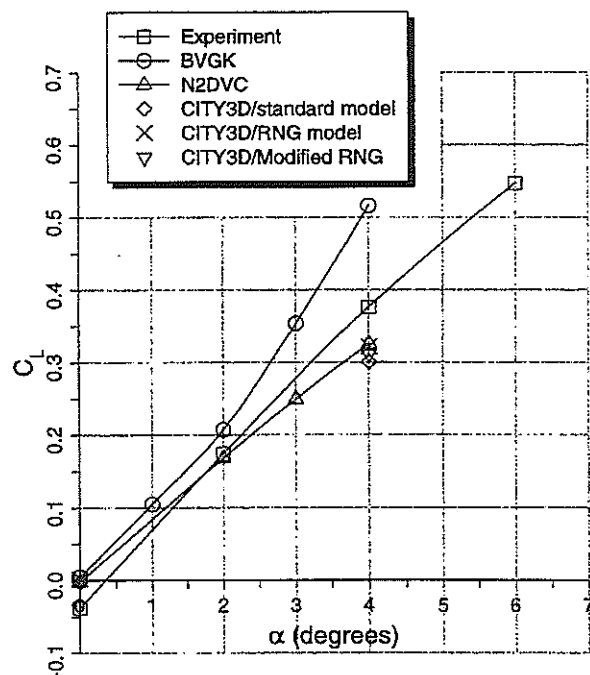

Figure 10. Comparison between the lift coefficients measured for the iced NACA 0012 aerofoil and values predicted by the CFD codes.

It can be seen from figure 11 that the BVGK drag coefficient predictions show poor agreement with the experimental results at all incidences. It was found that there were large discrepancies between the pressure distribution around the faired aerofoil and the pressure distribution measured by experiment (Ref. 6), especially around the leading edge. In view of the relatively accurate results predicted by BVGK for the clean aerofoil, the large discrepancies observed between the BVGK and experimental results for the iced aerofoil suggest that the modified aerofoil geometry is not a valid representation of the original accretion. Since these modifications were necessary to allow BVGK to converge and produce a flow solution, it is clear that the capability of BVGK for predicting flow around this geometry is poor. Ice

accretions will frequently have similar geometries to the simulated ice shape chosen for this investigation, with large areas of separated flow. It is therefore concluded that BVGK has a very limited capability for analysing the aerodynamic performance of iced aerofoils in its present stage of development. Further discussions will be needed with the code developers to establish whether any modifications could be made to improve its application to iced aerofoils.
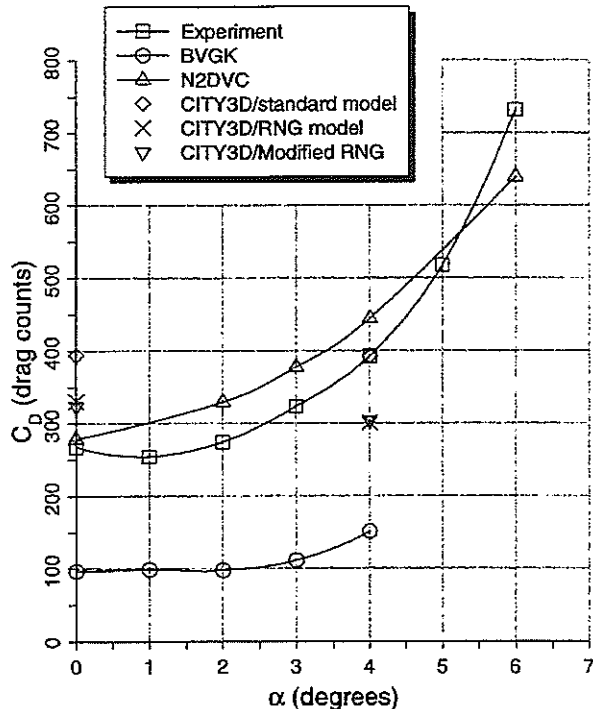

Figure 11. Comparison between the drag coefficients measured for the iced NACA 0012 aerofoil and values predicted by the CFD codes.

N2DVC Results

Grid Generation

N2DVC used a combination of an initial algebraic grid generator, followed by an elliptic generator which produced a smoothly varying, near-orthogonal grid. Finally, a Navier-Stokes grid was produced by redefining the normal distribution of grid points to allow a reasonable resolution of boundary layers and wakes.

A grid was generated around each of the two aerofoil sections (figure 12). Each grid was of C-type topology, consisting of 257 by 65 grid points, with 48 cells in the wake region downstream of the trailing-edge and 80 cells on each of the lower and upper surfaces. In the direction normal to each aerofoil section there were 64 cells with the cell height adjacent to the surface equal to 10^{-5} of the

clean aerofoil chord. Care was taken to cluster a sufficient number of points around the ice accretion, to represent accurately the regions of high surface curvature which occur at the lower and upper ice horns and at the junction of the ice with the clean aerofoil section.
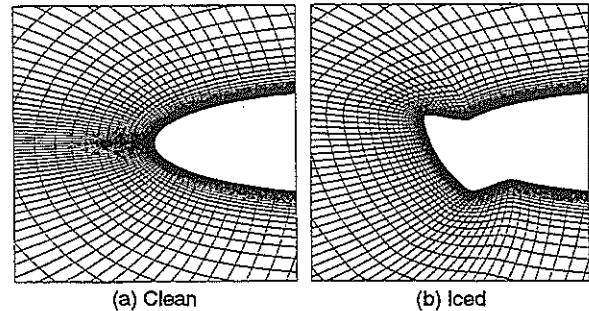

(a) Clean   (b) Iced

Figure 12. Grids used by N2DVC for the clean and iced NACA 0012 aerofoil.

Flow Calculations

A range of Navier-Stokes calculations was carried out using the two-dimensional Vertex-Centroid flow solver for the clean and iced aerofoil sections. The flow conditions used corresponded to the experimental investigation discussed by Bragg and Coirier (Ref. 6), namely a Mach number of 0.12 and a Reynolds number (based on the clean aerofoil chord) of 1.5×10^6. A range of angles of attack was chosen to correspond to the experiment, namely 0°, 2°, 4° and 6°. In addition, both aerofoil sections were assumed to be smooth. The transition position for the clean aerofoil section was fixed at 5% of chord to correspond to the experiment. For the simulated iced section, however, the experimental ice shape was tested with no transition strip and no distributed roughness. This presented a difficulty in performing a numerical calculation with the Baldwin-Lomax turbulence model in that the position of transition was unknown. This difficulty was compounded by the fact that the transition location is a function of angle of attack. Bragg and Khodadoust (Ref. 7) have found that the shear layers separating from the ice horns are in fact laminar, so that these are laminar separation bubbles. From an examination of momentum thickness and pressure recovery location they found that the free shear layers then undergo transition to turbulence. The turbulent shear layer then entrains high energy external flow allowing pressure recovery and re-attachment to occur. The position of shear layer transition and re-attachment depends upon angle of attack. Because of the difficulty in determining transition position, the calculations for the iced aerofoil section were initially made assuming that the flow was fully turbulent. Thus, the separations from the ice horns were modelled as turbulent boundary layer separations. Some further calculations to determine the sensitivity to transition location are discussed later.
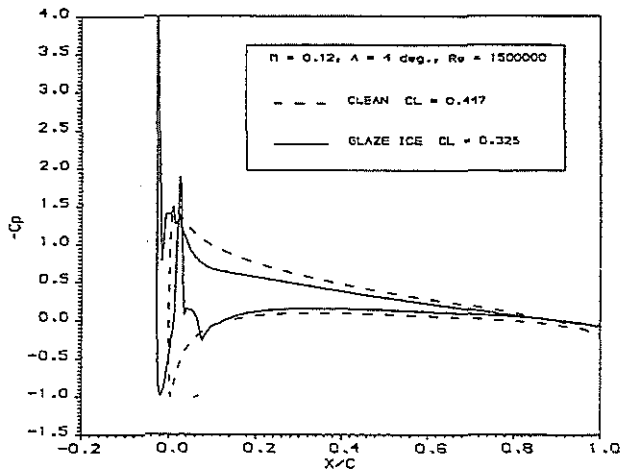
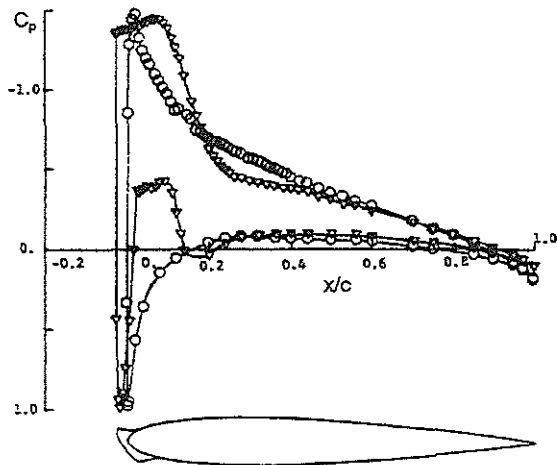Figure 13. Surface pressures computed by N2DVC for the NACA 0012 aerofoil at $\alpha = 4°$.

Figure 14. Surface pressures measured by experiment for the iced NACA 0012 aerofoil at $\alpha = 4°$ (taken from Ref. 6)

The calculated surface pressure coefficient plots for the clean and simulated glaze ice aerofoils are shown in figure 13 for the $\alpha = 4°$ case. For the glaze ice section, the approximate location of separation from the lower and upper ice horns is marked by a very large pressure spike. This is in marked contrast to the experimental surface pressures where no pressure spikes are evident (figure 14). However, the computations qualitatively resemble the experiment in that, behind the separations, small, approximately constant, pressure plateaux are seen. These are followed by a relatively strong pressure recovery, with a more moderate pressure recovery towards the trailing-edge. The computations differ from the experiment in the suction levels of these pressure plateaux and in their width and location. Although the computed suction level compares well with the experimental upper surface pressure

plateau for the 4° case, the agreement was worse at 2° and 6°. Furthermore, the code under-predicted the width of the suction level of this pressure plateau at all incidences. Discrepancies also exist between the computed lower surface pressure plateau and the experimental measurements.

With the exception of the 0° case, fully converged steady values of the lift and pressure drag for the iced computations could not be obtained. For the 2° and 4° cases, the pressure drag and lift coefficients converged to a steady oscillatory behaviour but with a well defined mean value. Figure 15 shows this convergence behaviour for the 4° case. For the 6° case, the pressure drag and lift were again highly oscillatory, with the pressure drag having a well defined mean value, but not the lift coefficient. Khodadoust (Ref. 10) reports that the bubble at 6° and above is extremely unsteady, and likely to be burst some percentage of the time. This may be reflected in the difficulty in obtaining a steady numerical solution for this case. It was found that the oscillations in pressure drag and lift coefficients for all cases were caused by an oscillation in the upper surface pressures along the entire upper surface of the aerofoil, beginning at the base of the large pressure spike on the upper surface. Interestingly, the skin friction drag coefficients appeared to converge to steady values but much lower in magnitude than those of the pressure drag.
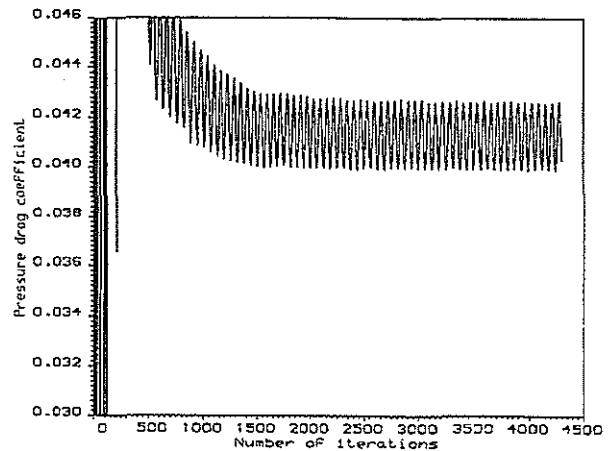

Figure 15. Pressure drag convergence for the iced aerofoil at $\alpha = 4°$.

The computed and experimental lift and drag coefficients for the clean and iced aerofoil sections are compared in figures 7, 8, 10 and 11, using mean values for solutions that were oscillatory. There is excellent agreement between the computed and experimental lift and drag coefficients for the clean aerofoil with fixed transition (fig. 7 and 8). For the iced aerofoil section, the computations show a significant increase in the drag coefficient compared to the clean section, with this difference becoming greater with incidence (fig. 10). There is also a marked reduction in lift coefficient compared to the

clean aerofoil. For the iced section, however, the computed lift coefficients are in general too low compared to experiment, becoming progressively lower with increasing incidence. The drag coefficients are approximately 50 drag counts too high, except for the 6° case where the drag is approximately 100 counts lower than in the experiment. The validity of this latter result remains questionable, however, as the lift coefficient has not converged to a stable behaviour.

The differences between the numerical computations and the experiment, together with the apparent unsteadiness of the flow (even for the lower angles of attack) were sufficient that it was decided to repeat some of the calculations ($\alpha = 2°$ and 4°) for the iced aerofoil on a finer grid. This had 513 by 129 grid points, with 48 cells in the wake region as before, but 208 cells on each of the lower and upper surfaces, and 128 cells in the direction normal to the surface. The higher density of grid points in the region of the glaze ice shape allowed a much higher resolution of the free shear layers and the structure of the re-circulating bubbles. The surface pressure coefficients using the fine grid are compared with those using the original grid in figure 16. The pressure spikes are still present, although they are slightly narrower and have reduced in magnitude. The width of the upper surface pressure plateau has increased and is in better agreement with the experiment. In addition, the pressure recovery region has moved further downstream.
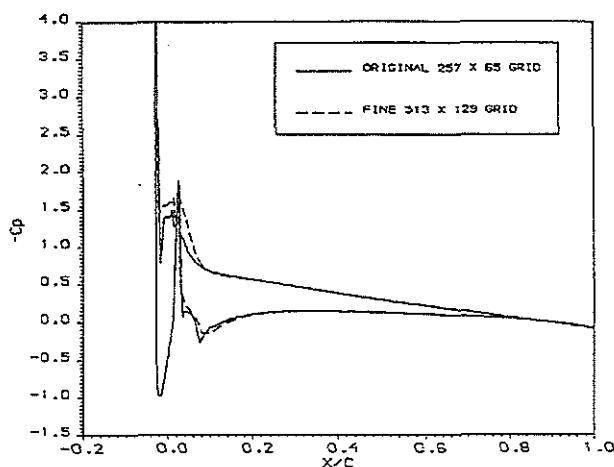

Figure 16. Comparison of predicted surface pressures using the original and fine grid at $\alpha = 4°$.

Using the fine grid, the convergence behaviour was much better with no oscillations for the cases tested ($\alpha = 2°$ and 4°). It was also observed that the lift and drag coefficients calculated using the finer gird were considerably closer to the values measured by experiment (Table 2). However, this is somewhat misleading considering that the surface pressures are still significantly different.

Further calculations were made for the 2° and 4° cases to investigate the sensitivity of the transition location on the computational results. Using the original grid, the effect of moving the transition to 5% chord was to increase the suction levels of the upper and lower pressure plateaux and move these features further downstream. The pressure spikes were only slightly reduced in magnitude. The drag coefficient was slightly reduced, although not by as much as was obtained by refining the grid (Table 2). The lift coefficient increased further from the experimental value.
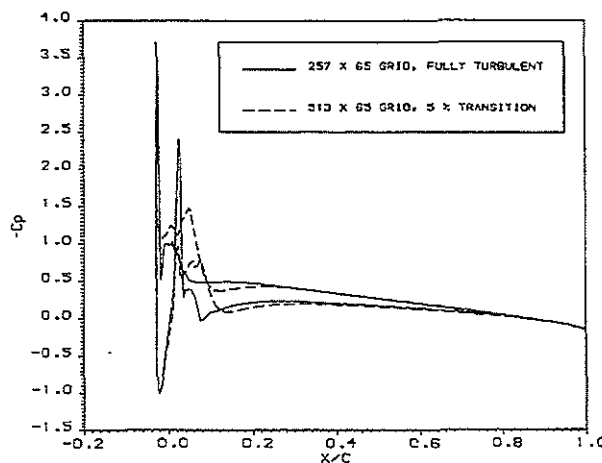

Figure 17. Comparison of predicted surface pressures using different transition locations ($\alpha = 2°$).

Calculations were repeated at 2° with the transition location again set at 5% but this time the fine grid was used. The surface pressures are shown in figure 17. Here, the suction levels and width of the pressure plateaux have increased significantly. In addition, the ends of the strong pressure recovery regions have moved significantly closer to the experiment. It may also be observed that the magnitude of the pressure spikes have been considerably reduced, with the one on the lower surface almost non-existent. Consequently, the drag coefficient has moved significantly closer to the experiment although the lift coefficient has increased to a higher value (Table 2).

The effect of refining the grid and moving the transition location back to 5% for the 2° case is shown in figure 18. Here we see that moving the transition to 5% chord or refining the grid both have the effect of increasing the size of both lower and upper surface bubbles, with the resultant re-attachment points moving further downstream. The combined effect of both refining the grid and of moving the transition to 5% is quite dramatic. The size of the re-circulating regions on both surfaces has increased. The upper surface region, however, now appears to consist of two contra-rotating re-circulating bubbles.

α	C_L					C_D (drag counts)				
(degrees)	Exp.	Original grid		Fine grid		Exp.	Original grid		Fine grid	
		Fully turbulent	5% transition	Fully turbulent	5% transition		Fully turbulent	5% transition	Fully turbulent	5% transition
2	0.174	0.168	0.194	0.185	0.206	274	329	316	295	297
4	0.376	0.325	n/c	0.348	n/c	392	444	n/c	395	n/c

n/c = not computed

Table 2.   Effect of grid refinement and transition location on the lift and drag coefficients for the iced aerofoil computed by N2DVC.
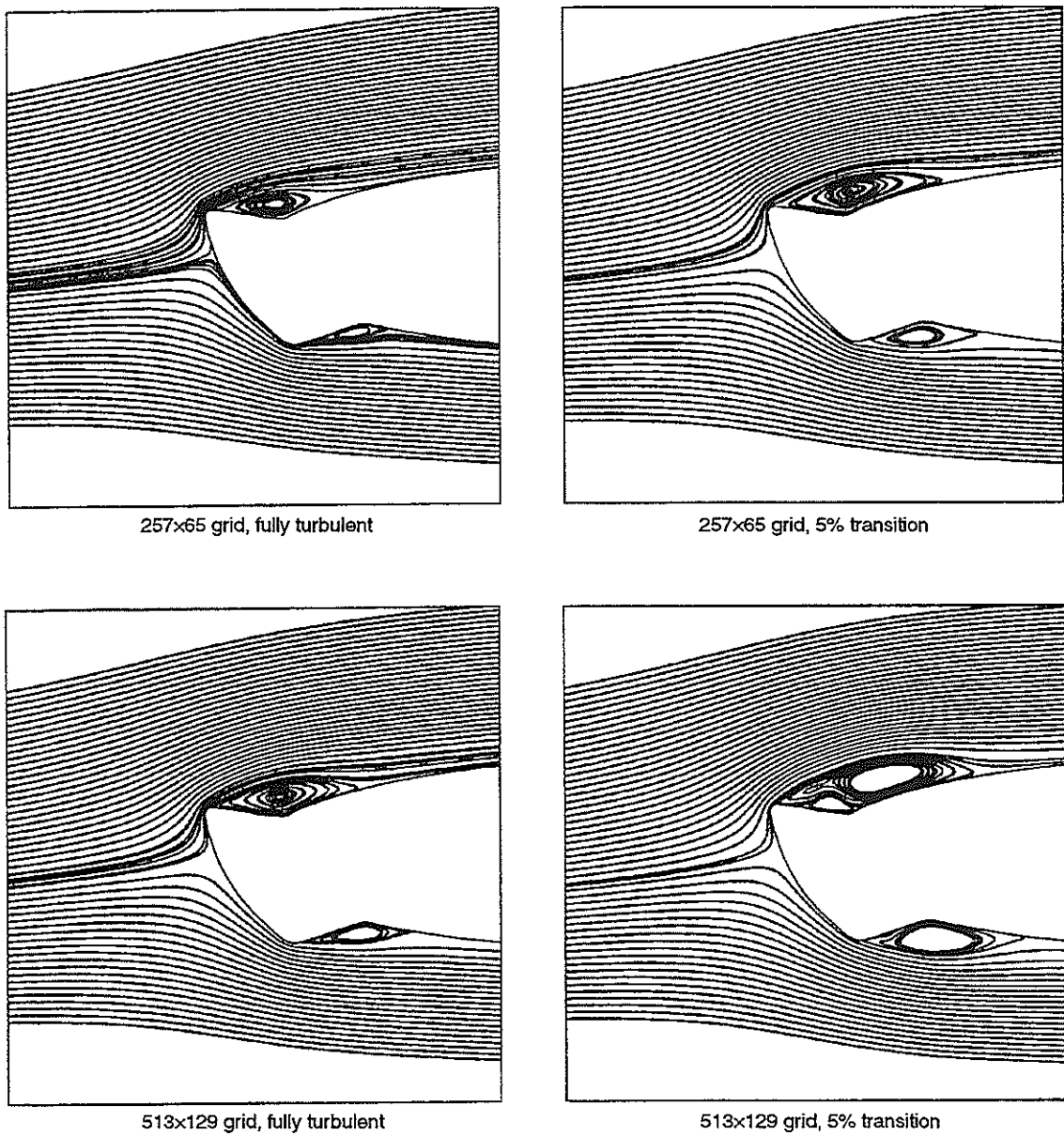

257x65 grid, fully turbulent

257x65 grid, 5% transition

513x129 grid, fully turbulent

513x129 grid, 5% transition

Figure 18.   Effect of the grid refinement and transition location on the computed flowfield

CITY3D Results

Calculations with the CITY3D code were limited to incidences of 0° and 4°. Results are shown in figures 10 and 11 respectively.

For the $\alpha = 0°$ case, the computed force coefficients are very sensitive to the choice of the discretisation scheme. Thus, for example, the predicted pressure drag coefficient is 0.0488 with the Upwind scheme but is 0.0337 with the MINMOD scheme. These results suggest that further grid refinement may be needed to obtain truly grid-independent simulations. The computed drag coefficient is moderately sensitive to the choice of turbulence model: a value of 0.0393 is obtained for the standard k-ε model compared to 0.0330 obtained with the RNG formulation. The RNG result is closer to the measured value of 0.0267 and this suggests that further improvements may be obtained from using the more refined Reynolds-stress closure. There is almost no significant sensitivity to the assumed turbulence levels at inlet: a pressure drag value of 0.0286 is obtained for the high turbulence-intensity level while the low intensity calculations yield a value of 0.0281.

For the $\alpha = 4°$ case, two very different but logical treatments of the inlet/outlet boundary conditions, namely the RNG and modified RNG formulation, yielded essentially identical drag coefficient values of 0.0300 and 0.0303 respectively. A much greater sensitivity to the choice of turbulence model is observed for this case; the standard k-ε model predicts C_D to be 0.0392, exactly equal to the experimentally measured value, while the RNG formulation gives a value of 0.0303. The apparent accuracy of the standard k-ε model may be fortuitous, however, in view of the significantly less accurate drag coefficient prediction for the $\alpha = 0°$ case. The computed results suggest that the code is somewhat insensitive to changes in incidence, although its true accuracy is difficult to quantify given the limited number of test results, and more research is required for a true evaluation to be obtained.

It is very likely that the computations for the 4° case are especially sensitive to grid effects. This is owing to the large separated flow region and consequent skewing of the streamlines relative to the grid lines. Another possible cause for discrepancy between predictions and measurements is the assumption, in the predictions, of turbulent flow everywhere within the computational domain. No allowance is made for the possibility of a laminar boundary layer developing over the iced portion of the aerofoil. The prediction of laminar-turbulence transition is beyond the capabilities of all known advanced turbulence models and can only be achieved, at present, by empirical adjustment to zero-equation closures. Further work in this area may include the use of a low Reynolds-number turbulence closure so that the assumption of the existence of a fully-turbulent log-law region may be dispensed with.

Conclusions

The capability of current CFD codes to analyse iced aerofoil performance has been assessed. Several CFD programs have been used to evaluate the aerodynamic characteristics of a NACA 0012 aerofoil with a simulated glaze ice accretion and the results have been compared against experimental data.

The flow around an aerofoil with glaze ice at the leading-edge is an extremely complicated one. The presence of large re-circulating regions coupled with free-shear layer transition and inherent unsteadiness make this an extremely challenging area of application for computational fluid dynamics. It has been concluded that a viscous-inviscid interaction CFD code such as BVGK is not suitable for predicting the flow around iced aerofoils. This method is not currently capable of calculating the large separation bubbles that develop around ice accretions, and will therefore not predict the significant drag increases that arise from the formation of ice on aerofoils.

The Navier-Stokes flow solvers assessed during this investigation have provided more accurate results when compared with the experimental data. However, calculations made by N2DVC in this report have shown the high sensitivity of the calculated flow to a variety of factors such as grid refinement and the location of transition. The detailed structure of the re-circulating regions has a significant effect on the computed surface pressures and hence on the lift and drag coefficients. Initial results from CITY3D, the unsteady Navier-Stokes code, have also shown that significantly different results are obtained by employing various numerical schemes and turbulence models within the flow solver.

The application of an equilibrium turbulence model such as a Baldwin-Lomax model to a flow containing large re-circulating bubbles and free-shear layer transition is questionable. In addition, there is strong experimental evidence that these bubbles are unsteady for at least part of the time which calls into question the use of a steady flow solver, especially for higher angles of attack. All of these limitations preclude such a method from being a useful tool at angles of attack approaching stall and hence for determining maximum lift coefficient for aerofoils with glaze icing. Further studies analysing the performance of iced aerofoils should therefore be performed using unsteady flow solvers.

There is a need to investigate and implement code modifications to model the surface roughness of ice accretions, to allow aerofoils with real ice accretions

to be assessed. Before further work can be undertaken, a more robust grid generator must be found. Even if an effective CFD analysis is established for the smoothed ice shape, the modelling of a truly representative ice shape with typical irregularities and surface roughness sets a further, more difficult challenge.

Acknowledgement

References

1. Course notes from the University of Kansas, Aerospace Short Course: "Aircraft icing: Meteorology, protective systems, instrumentation and certification", Seattle, April 1996, pp11.5.

2. Gent, R.W., "An empirical based method for the prediction of helicopter power increase during flight in icing weather conditions", DERA unpublished work, 1994.

3. Ashill, P.R., Woods, R.F., and Weeks, D.J., "An improved semi-inverse version of the Viscous Garabedian and Korn method (VGK)", RAE Report, January 1987.

4. O'Brien, P., "An accurate and robust method for calculating viscous flows: Final report", DERA unpublished work, 1996.

5. Collyer, M.R., "An extension to the method of Garabedian and Korn for the calculation of transonic flow past an aerofoil to include the effects of a boundary layer and wake", RAE Report, July 1977.

6. Bragg, M.B. and Coirier, W. J., "Aerodynamic measurements of an airfoil with simulated glaze ice", in "AIAA 24th Aerospace Sciences Meeting", Reno, Nevada, January 1986, paper AIAA-86-0484.

7. Bragg, M.B. and Khodadoust, A., "Measurements in a large separation bubble due to a simulated airfoil ice accretion", AIAA Journal Volume 30, No. 6, June 1992, pp 1462-1467.

8. Bragg, M.B. and Khodadoust, A., "Experimental measurements in a large separation bubble due to a simulated glaze ice accretion", in "AIAA 26th Aerospace Sciences Meeting", Reno, Nevada, January 1988, paper AIAA-88-0116.

9. Potapczuk, M., "Numerical analysis of a NACA 0012 aerofoil with leading edge ice accretions", in "AIAA 25th Aerospace Sciences Meeting", Reno, Nevada, January 1987, AIAA-87-0101.

10. Khodadoust, A., "A flow visualisation study of the leading edge separation bubble on a NACA 0012 aerofoil with simulated glaze ice", M.S. Thesis, Ohio State University, Colombus, Ohio, June 1987; also NASA CR 180846, January 1988.